

Selective Molecular-Gating Adsorption in a Novel Copper-Based Metal-Organic Framework

Atsushi Kondo,^{a*} Taiki Yashiro,^a Naoya Okada,^a Shotaro Hiraide,^b Takahiro Ohkubo,^c Hideki Tanaka^b and Kazuyuki Maeda^{a*}

a. Tokyo University of Agriculture and Technology, 2-24-16 Naka-cho, Koganei, Tokyo, 184-8588 Japan.

b. Department of Chemical Engineering, Kyoto University, Nishikyo, Kyoto 615-8510, Japan.

c. Department of Chemistry, Graduate School of Natural Science and Technology, Okayama University, 3-1-1 Tsushima-naka, Kita-ku, Okayama 700-8530 Japan.

Contents

Figure S1. SEM images of **1** and the sample after guest exchange.

Figure S2. TG curves of **1** and **1h₄₇₃** from room temperature to 1073 K measured under N₂ flow of 150 mL/min.

Table S1. CHN elemental analysis of **1** and **1h₄₇₃**.

Figure S3. XRD patterns of **1**, **1h₃₇₃**, and **1h₄₇₃** at room temperature in air.

Figure S4. Synchrotron XRD patterns of **1** in a temperature range of 100 K - 473 K under vacuum and simulated XRD pattern of **1**.

Table S2. Thermal expansion coefficients of MODFs and Prussian blue complexes.

Figure S5. Adsorption isotherms of Ar (black circle) and O₂ (red square) at 77 K.

Figure S6. Molecular sizes of small alcohols.

Figure S7. Vapor adsorption selectivities estimated by IAST.

Table S3. Highest selectivities of some equimolar two-components mixed gases estimated by IAST.

Table S4. Results of liquid phase ternary alcohol mixture adsorption.

Figure S8. In situ synchrotron XRD patterns before and after gas/vapor loadings.

Figure S9. In situ XAFS spectra on the Cu-*K*-absorption edge.

Figure S10. Final Rietveld fitting results of in situ synchrotron XRD patterns on **1(MeOH)** and **1(EtOH)**.

Table S5. Crystallographic parameters of **1(MeOH)** and **1(EtOH)**.

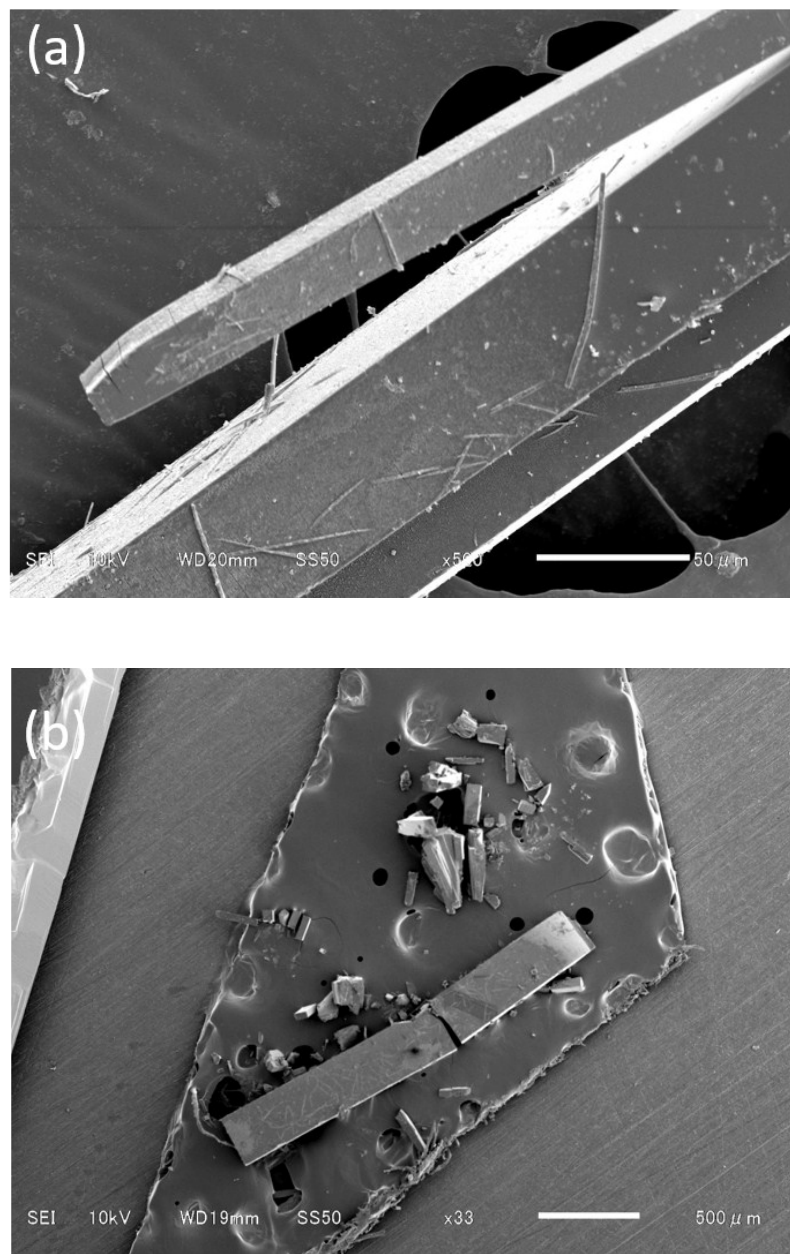


Figure S1. SEM images of (a) **1** and of (b) the sample after solvent exchange from acetonitrile to water put on a carbon tape.

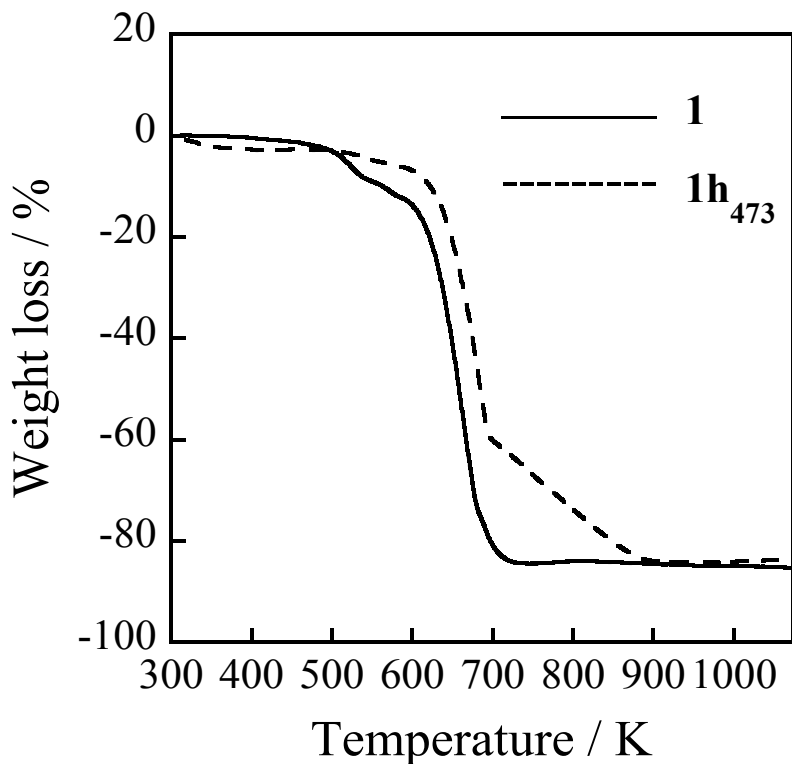


Figure S2. TG curves of **1** (solid) and **1h₄₇₃** (dotted) from room temperature to 1073 K measured under N₂ flow of 150 mL/min.

Table S1. CHN elemental analysis of **1** and **1h₄₇₃**.

		C / wt%	H / wt%	N / wt%
1	Obs.	47.48	2.84	19.29
	Calcd. ^a	47.69	3.00	19.46
1h₄₇₃	Obs.	44.47	2.68	17.42
	Calcd. ^b	44.42	2.76	17.27

^a The values were calculated for C₄₀H₃₀B₂F₈Cu₂N₁₄ (Estimated chemical formula of [Cu₂(tpt)₂(CH₃CN)₂]·2(BF₄)

^b The values were calculated for C₃₆H_{26.6}B₂F₈Cu₂N₁₂O_{2.6} (Estimated chemical formula of [Cu₂(tpt)₂(BF₄)₂]·4/3H₂O)

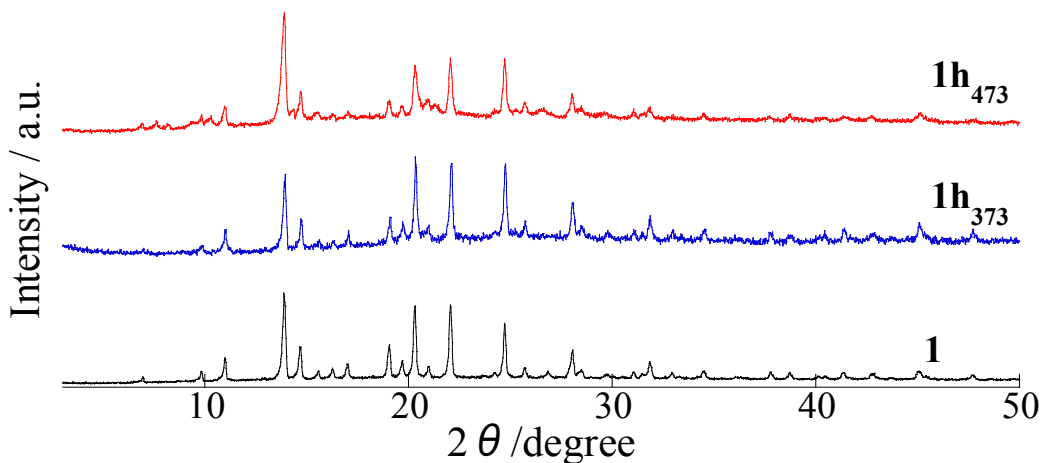


Figure S3. XRD patterns of **1**, 1h_{373} , and 1h_{473} at room temperature in air. The wavelength is 1.5418 Å.

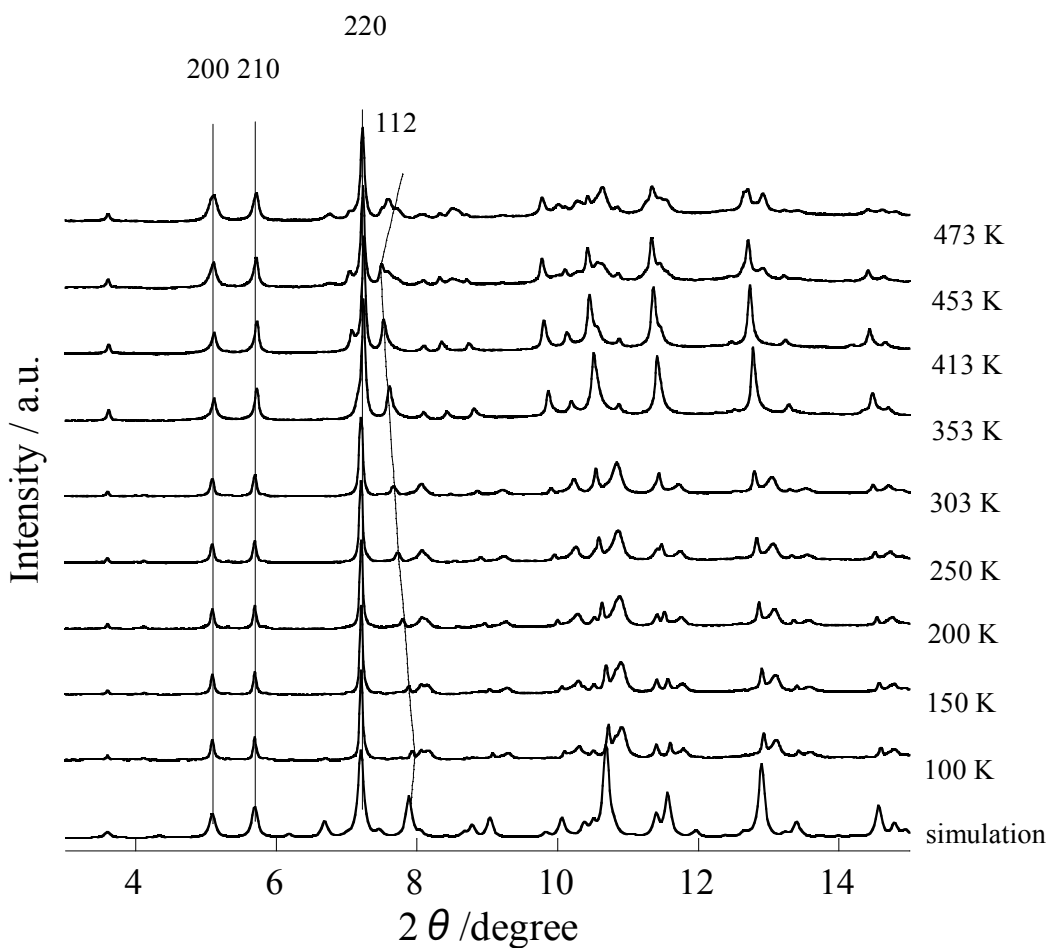


Figure S4. Synchrotron XRD patterns of **1** in a temperature range of 100 K-473 K under vacuum and simulated XRD pattern of **1** in the range of 3-15 (2θ/degree). In the heating process from 353 K to 473 K, the synchrotron

X-ray wavelength is 0.79942 Å, and in the cooling process from 303 K to 100 K, the wavelength is 0.79917 Å.

Table S2. Thermal expansion coefficients of some MOFs and Prussian blue complexes.

Materials	$\alpha_a / 10^{-6} \text{ K}^{-1}$	$\alpha_b / 10^{-6} \text{ K}^{-1}$	$\alpha_c / 10^{-6} \text{ K}^{-1}$	$\alpha_V / 10^{-6} \text{ K}^{-1}$	Reference
HKUST-1	-4.1	-4.1	-4.1	-11	1
MOF-5	-8	-8	-8	-24	2
[Zn(L ₁) ₂ (OH) ₂] ^a	-21	-21	127	89	3
H-MOF	177	-21	15	8	4
In[Ag(CN) ₂] ₃	105	105	-84	-	5
Ag ₃ [Co(CN) ₆]	130 ~ 150	130 ~ 150	-130 ~ -120	-	6
[Cu(OTf) ₂ (bpy) ₂]]	-21	-21	79	38	7
ZIF-7III	65 ~ 181	-124 ~ -110	95 ~ 141	47 ~ 197	8
ZIF-9III	128 ~ 255	-150 ~ -135	110 ~ 160	82 ~ 278	8
[Cu(BF ₄)(tpt) ₂] ^b	0.5	0.5	216	217	This work

$$\alpha_a = (a_{T_1} - a_{T_0})/(a_{T_0} \cdot (T_1 - T_0)), \alpha_b = (b_{T_1} - b_{T_0})/(b_{T_0} \cdot (T_1 - T_0)), \alpha_c = (c_{T_1} - c_{T_0})/(c_{T_0} \cdot (T_1 - T_0))$$

$$\alpha_V = (V_{T_1} - V_{T_0})/(V_{T_0} \cdot (T_1 - T_0))$$

a. L₁ = 4-(1H-naphtho[2,3-di]imidazol-1-yl)benzoate, b. tpt = 2,4,6-tri(4-pyridyl)-1,3,5-triazine

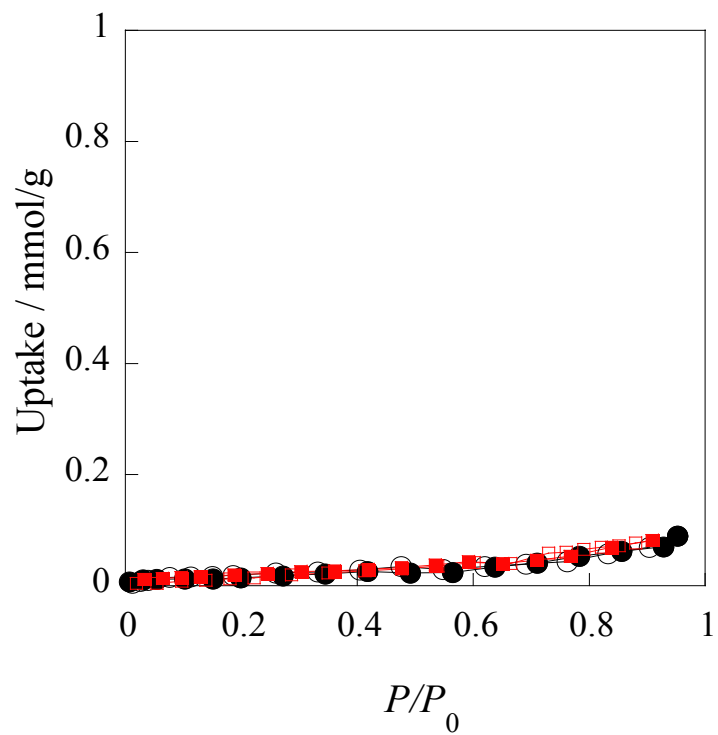


Figure S5. Adsorption isotherms of Ar (black circle) and O_2 (red square) at 77 K on **1a**. Filled and open symbols represent adsorption and desorption, respectively.

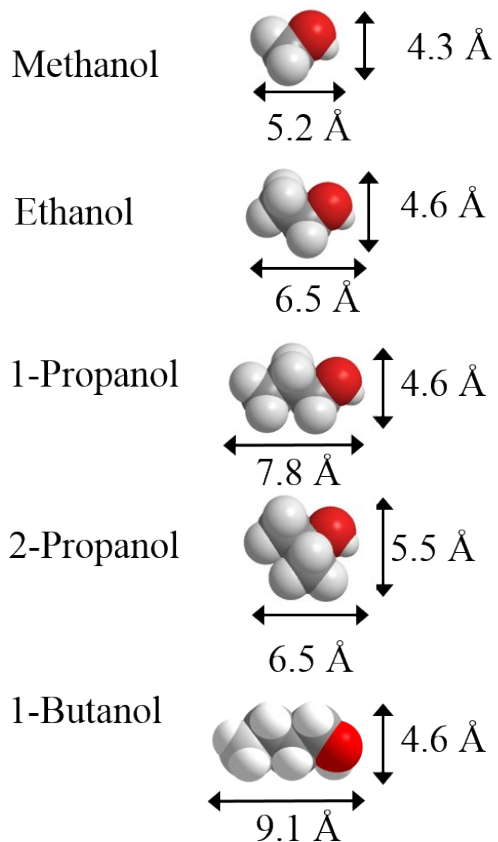
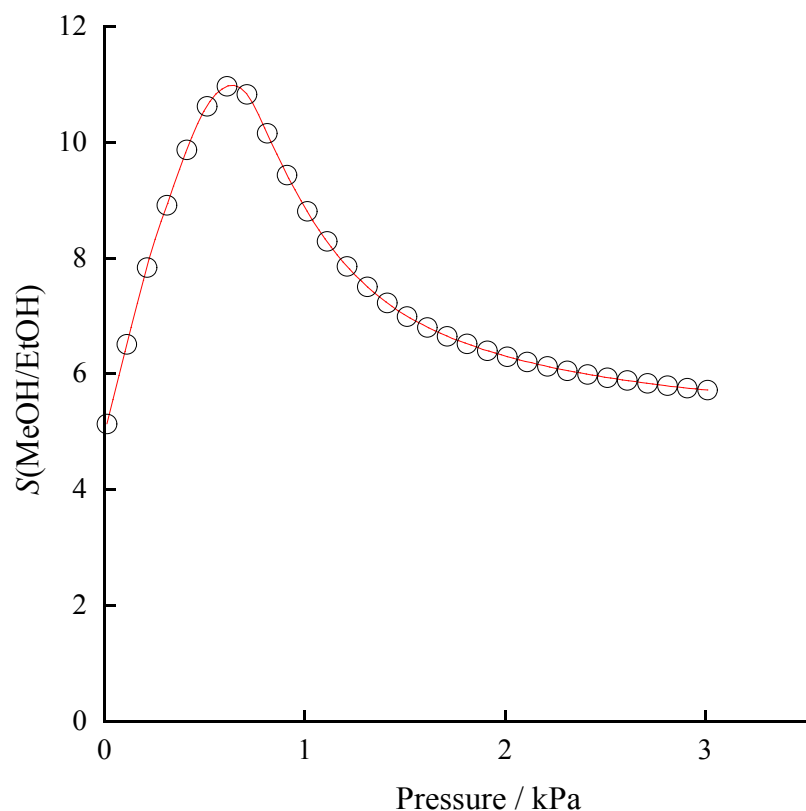
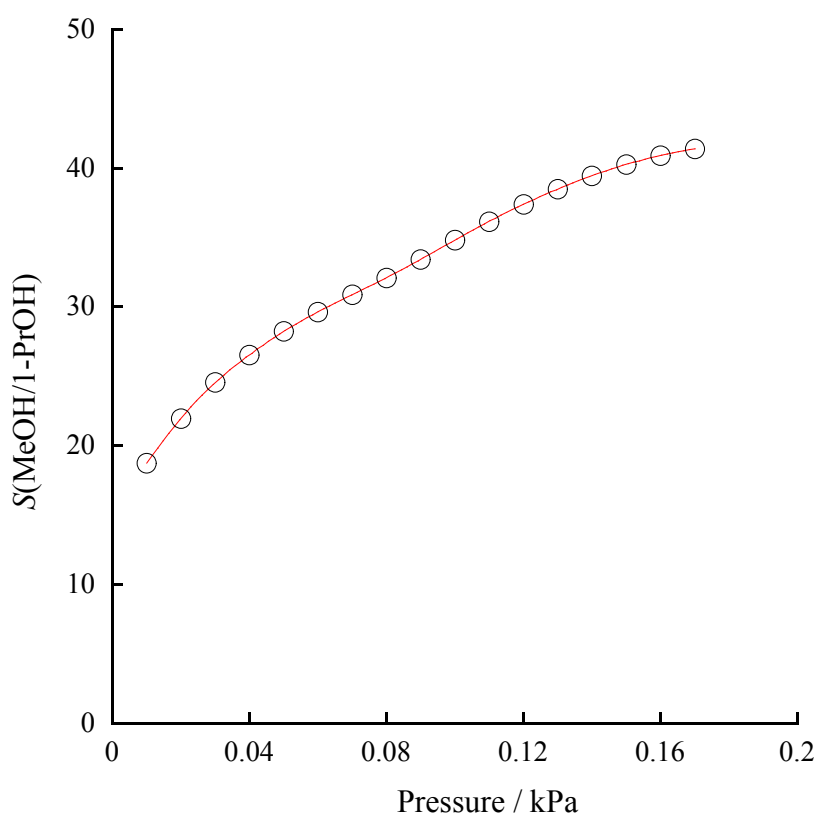


Figure S6. Molecular sizes of small alcohols.

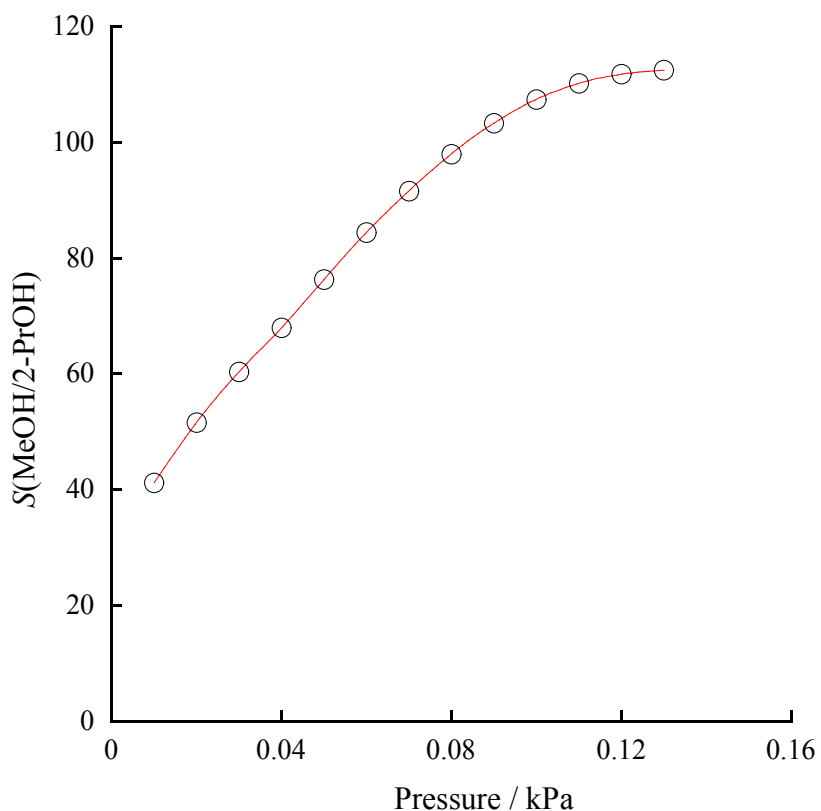
(a)



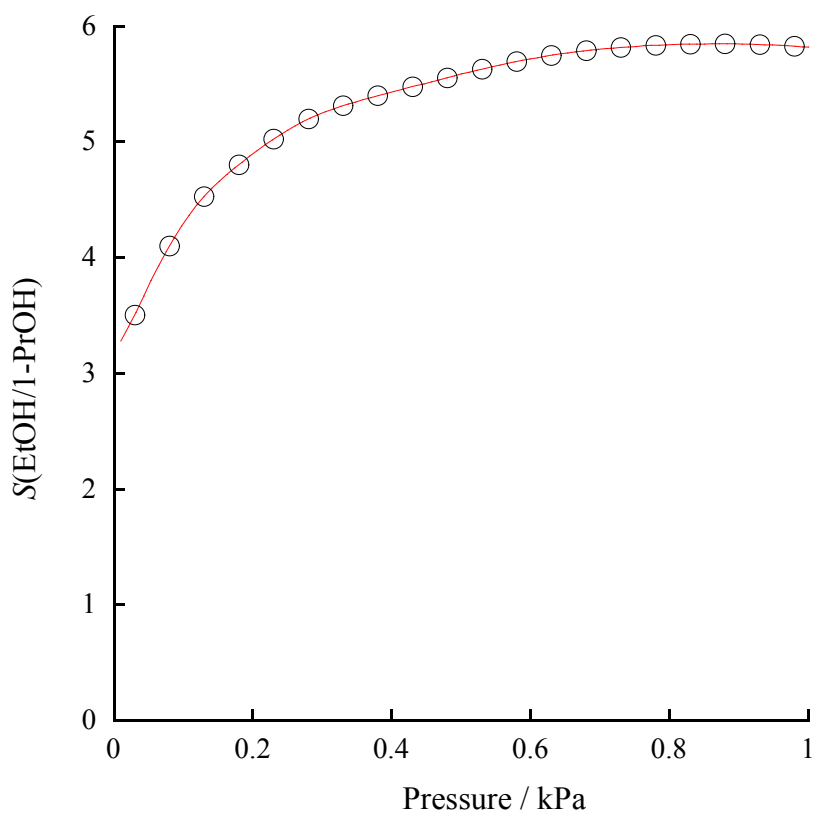
(b)



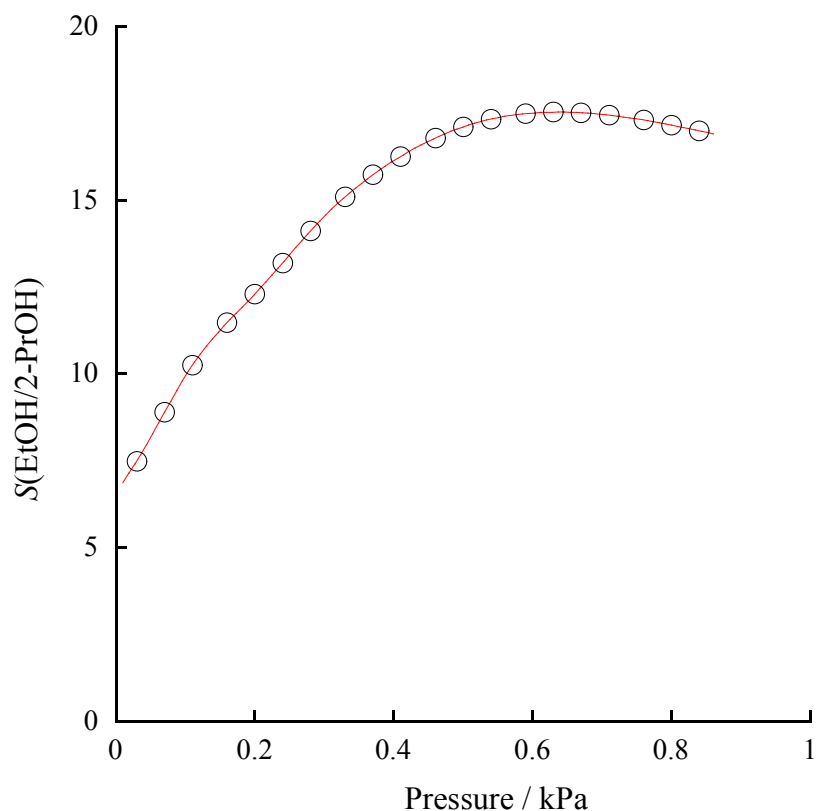
(c)



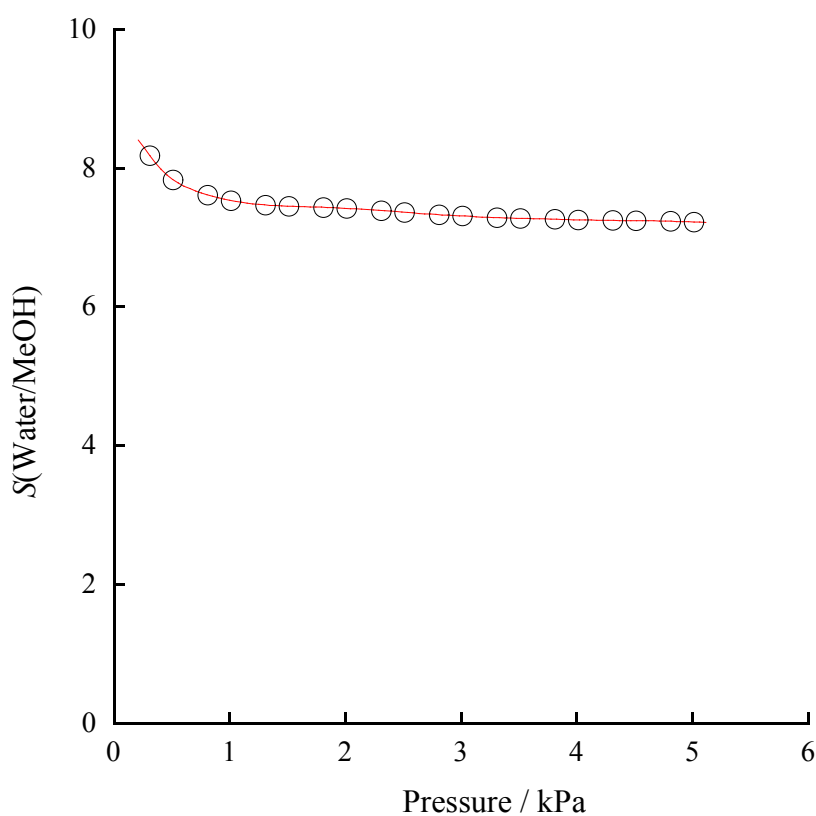
(d)



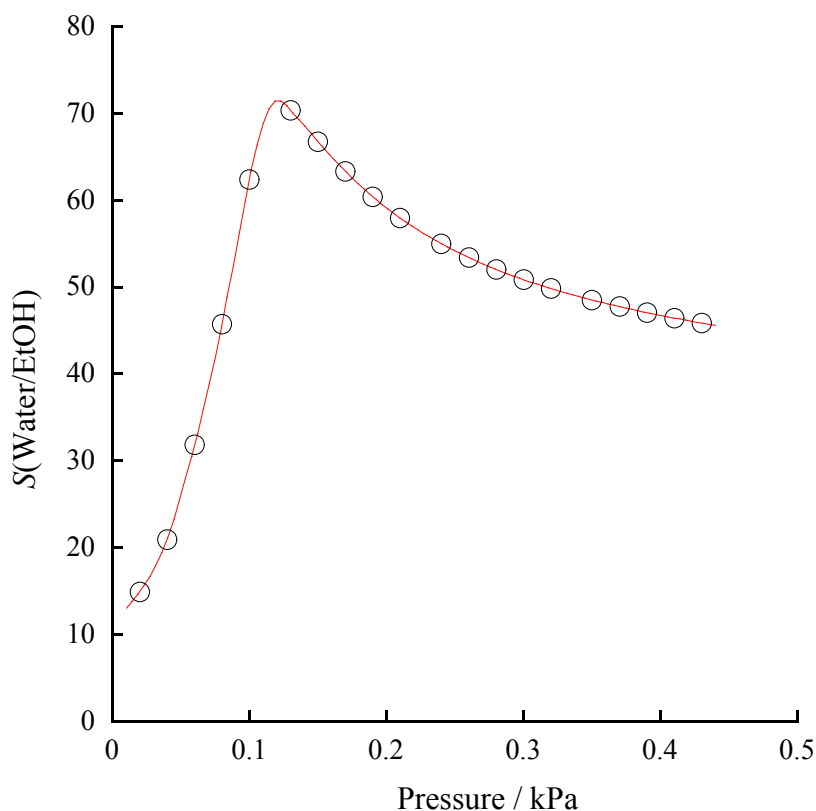
(e)



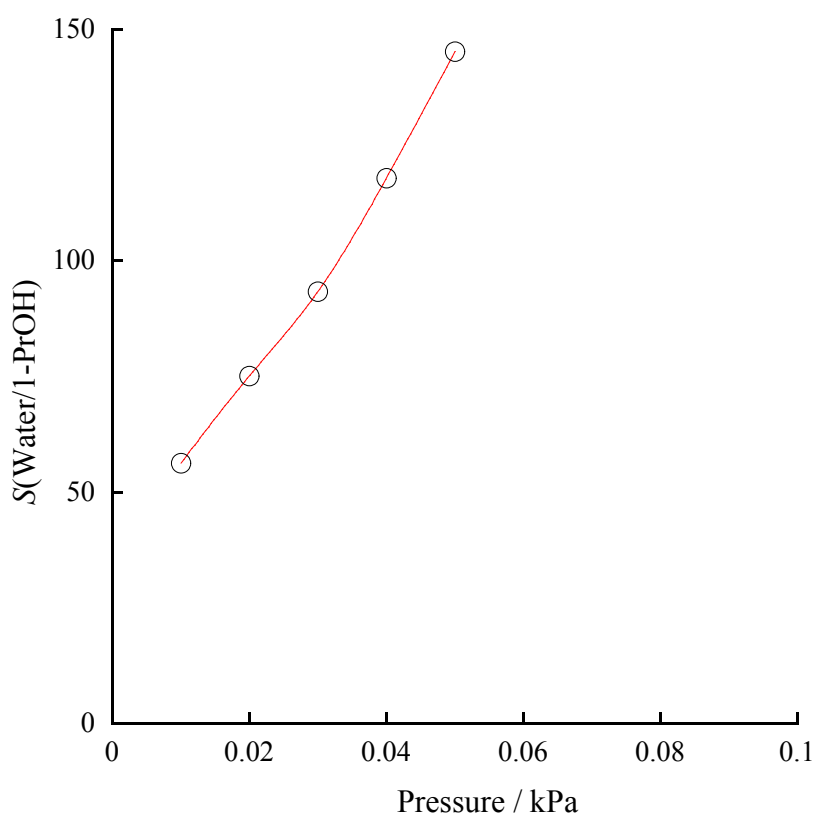
(f)



(g)



(h)



(i)

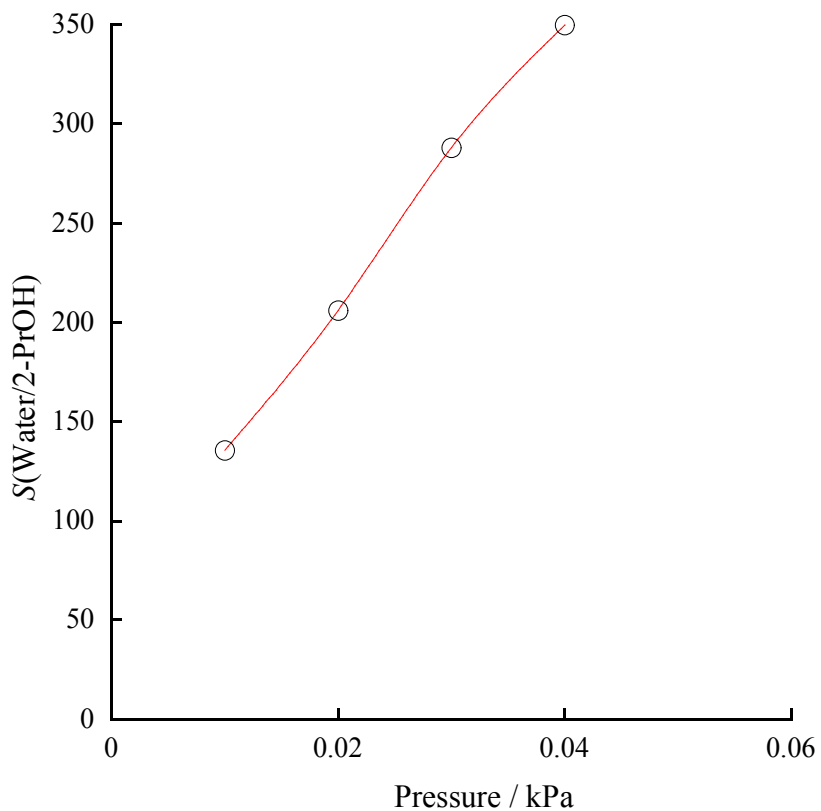


Figure S7. Vapor adsorption selectivity of (a) $S(\text{methanol/ethanol})$, (b) $S(\text{methanol/1-propanol})$, (c) $S(\text{methanol/2-propanol})$, (d) $S(\text{ethanol/1-propanol})$, (e) $S(\text{ethanol/2-propanol})$, (f) $S(\text{water/methanol})$, (g) $S(\text{water/ethanol})$, (h) $S(\text{water/1-propanol})$, (i) $S(\text{water/2-propanol})$ estimated by IAST.

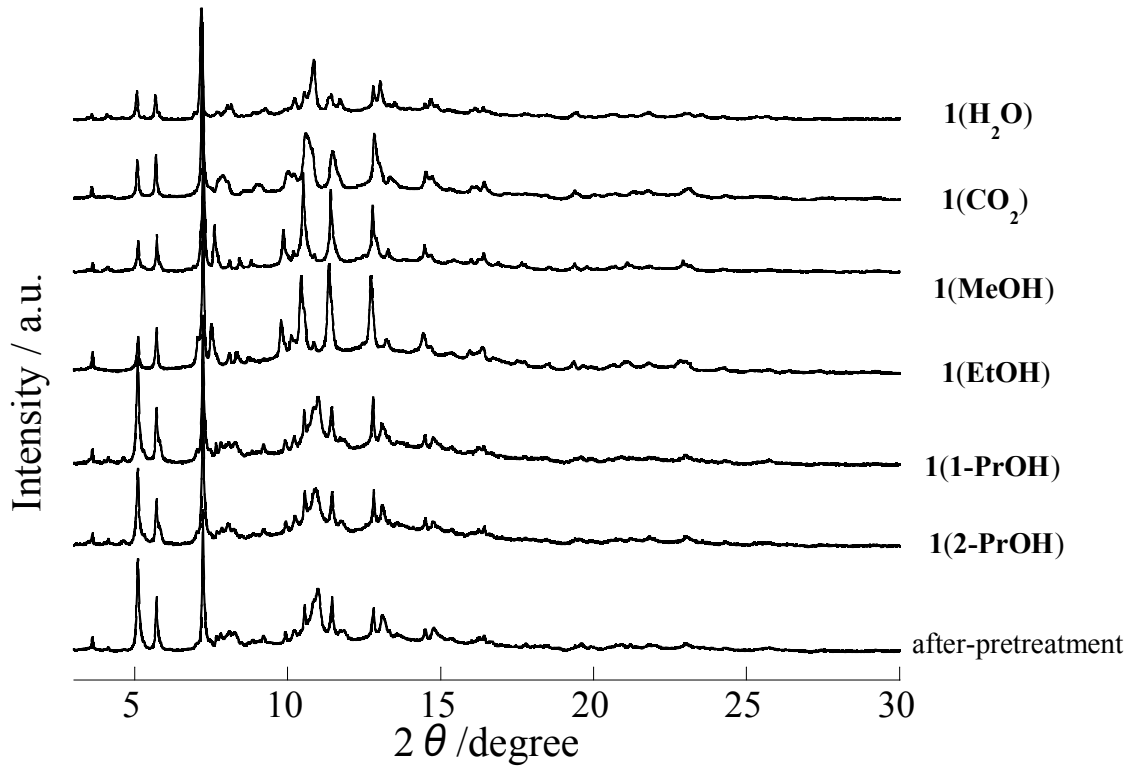
Table S3. Highest selectivities of some equimolar two-components mixed gases estimated by IAST. The values in parentheses are expected concentration percentages by one adsorption/separation process.

$S(\text{methanol/ethanol})$	$S(\text{methanol/1-propanol})$	$S(\text{methanol/2-propanol})$
11 (91.6 %)	41.4 (97.6 %)	112 (99.1 %)
$S(\text{ethanol/1-propanol})$	$S(\text{ethanol/2-propanol})$	$S(\text{H}_2\text{O}/\text{methanol})$
5.8 (85.4 %)	17.5 (94.6 %)	8.4 (89.3 %)
$S(\text{H}_2\text{O}/\text{ethanol})$	$S(\text{H}_2\text{O}/\text{1-propanol})$	$S(\text{H}_2\text{O}/\text{2-propanol})$
71.5 (98.6 %)	145 (99.3 %)	350 (99.7 %)

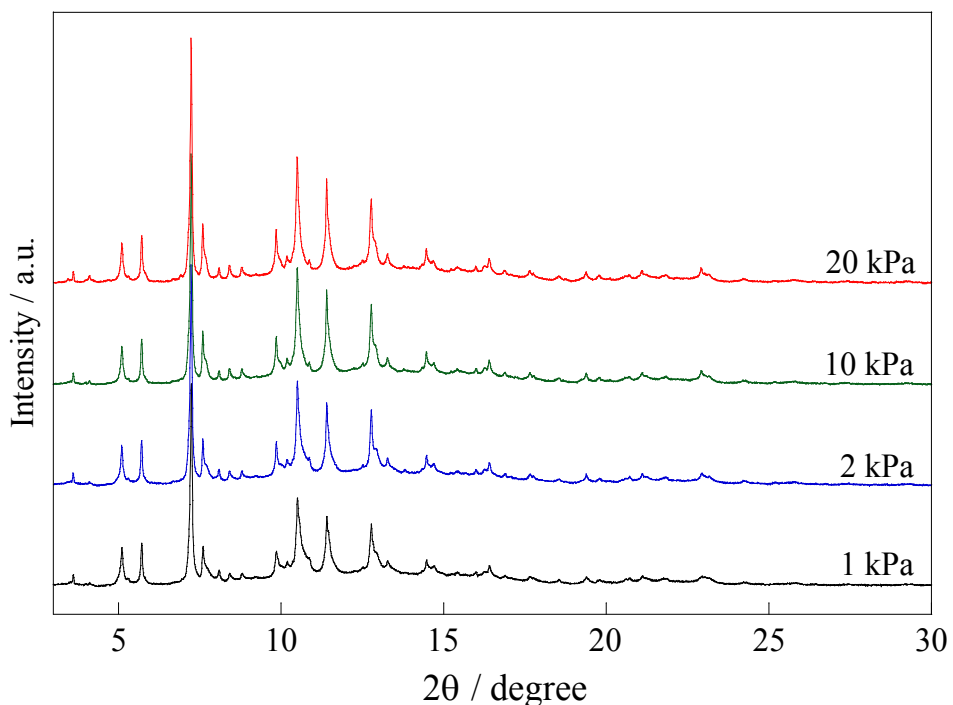
Table S4. Results of liquid phase ternary alcohol mixture adsorption.

Alcohol mixture	Initial relative amount against 1-butanol	Relative amount against 1-butanol after adsorption	Selectivity
Methanol 0.5 ml	0.13	0.092	$\sim 3.5 (S_{\text{MeOH/EtOH}})$
Ethanol 0.5 ml	0.087	0.080	
1-Butanol 9 ml	1	1	
Methanol 0.5 ml	0.13	0.11	$\sim 61 (S_{\text{MeOH/1-PrOH}})$
1-Propanol 0.5 ml	0.068	0.068	
1-Butanol 9 ml	1	1	
Methanol 0.5 ml	0.13	0.090	$\sim 80 (S_{\text{MeOH/2-PrOH}})$
2-Propanol 0.5 ml	0.066	0.066	
1-Butanol 9 ml	1	1	
Ethanol 0.5 ml	0.087	0.085	$\sim 5.7 (S_{\text{EtOH/1-PrOH}})$
1-Propanol 0.5 ml	0.068	0.068	
1-Butanol 9 ml	1	1	

(a)



(b)



(c)

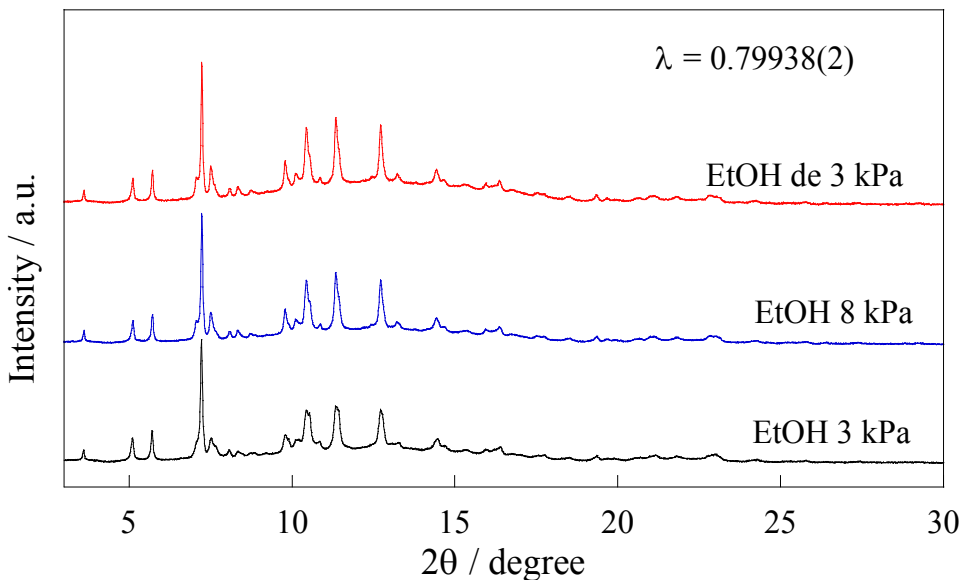


Figure S8. (a) In situ synchrotron XRD patterns of the MOF after the activation treatment (**1a**), **1(H₂O)**, **1(CO₂)**, **1(MeOH)**, **1(EtOH)**, **1(1-PrOH)**, and **1(2-PrOH)**. The wavelength was modified to be 0.79917 Å because **1(EtOH)** and **1(CO₂)** were measured with different wavelength (0.79942 Å). (b) In situ XRD patterns of **1(MeOH)** with several methanol gas loadings ($\lambda = 0.79917 \text{ \AA}$), and (c) in situ XRD patterns of **1(EtOH)** with several ethanol gas loadings ($\lambda = 0.79938 \text{ \AA}$). The XRD patterns were measured at 303 K except that with CO₂ gas (273 K).

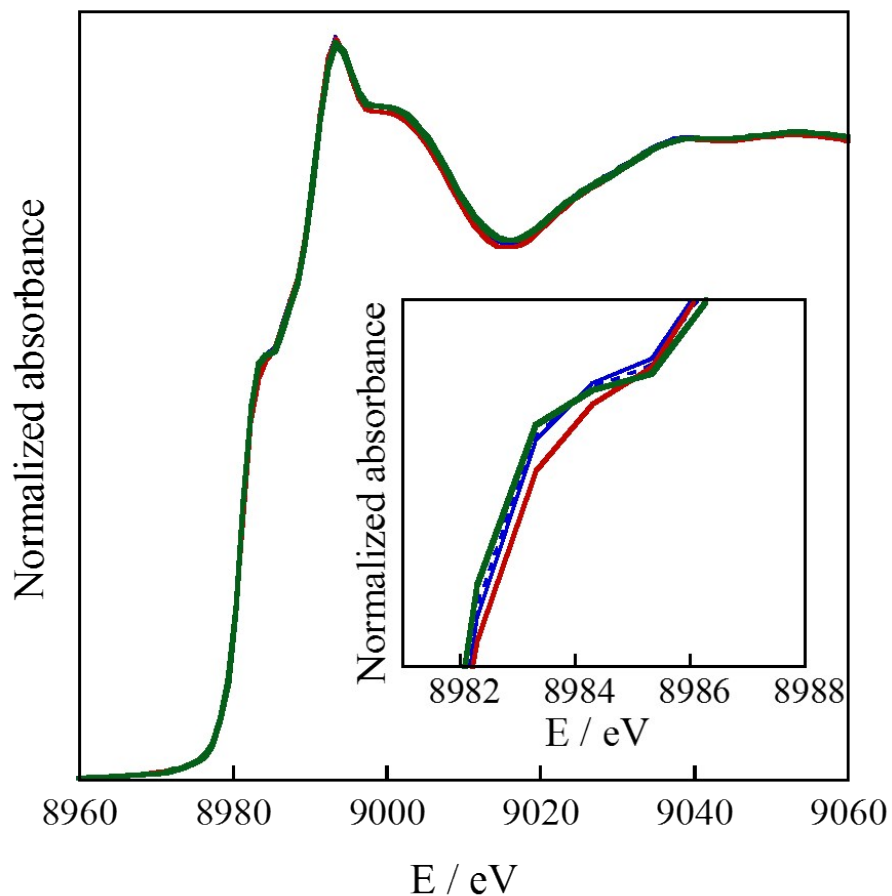


Figure S9. Local structure investigation around Cu(I) ion through vapor adsorption. Normalized Cu *K*-edge spectra of **1a** (green), **1(EtOH)** (brown), **1(1-PrOH)** (blue), and **1(2-PrOH)** (dotted blue). Inserted figure is enlarged one around 8983 eV.

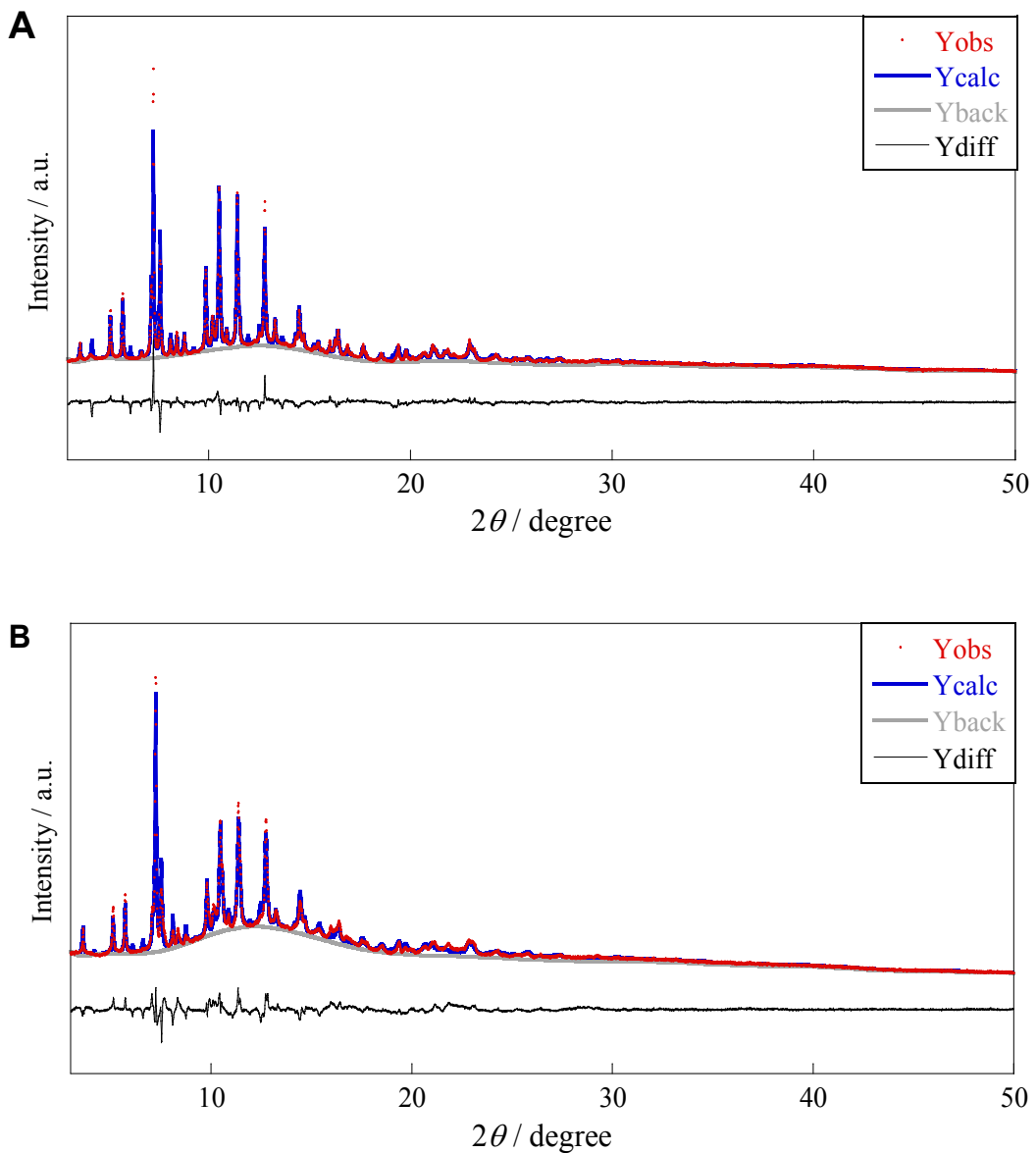


Figure S10. Final Rietveld fitting results of in situ synchrotron XRD patterns on (A) **1(MeOH)** ($R_p = 2.1\%$, $R_{wp} = 3.5\%$) and (B) **1(EtOH)** ($R_p = 2.5\%$, $R_{wp} = 3.7\%$). Synchrotron X-ray wavelength used is $0.79942(2)\text{ \AA}$.

Table S5. Crystallographic parameters of **1(MeOH)** and **1(EtOH)**.

	1(MeOH)	1(EtOH)
<i>Crystal system</i>	Tetragonal	Tetragonal
<i>Space group</i>	$P2_1c$	$P2_1c$
$a / \text{\AA}$	17.8698(6)	17.8866(10)
$c / \text{\AA}$	13.7392(10)	13.8782(20)
$V / \text{\AA}^3$	4387.3(3)	4440.0(6)
Z	4	4
T / K	303	303
$\lambda / \text{\AA}$	0.79942	0.79942
R_p	0.0021	0.0025
R_{wp}	0.035	0.037
R_F	0.050	0.083

Referemces

- (1) Y. Wu, A. Kobayashi, G. J. Halder, V. K. Peterson, K. W. Chapman, N. Lock, P. D. Southon, C. J. Kepart, *Angew. Chem. Int. Ed.*, **2008**, *47*, 8929-8932.
- (2) S. S. Han, W. A. Goddard III, *J. Phys. Chem. C*, **2007**, *111*, 15185-15191.
- (3) I. Grobler, V. J. Smith, P. M. Bhatt, S. A. Herbert, L. J. Barbour, *J. Am. Chem. Soc.*, **2013**, *135*, 6411-6414.
- (4) L. D. DeVries, P. M. Barron, E. P. Hurley, C. Hu, W. Choe, *J. Am. Chem. Soc.*, **2011**, *133*, 14848-14851.
- (5) J. L. Korčok, M. J. Katz, D. B. Leznoff, *J. Am. Chem. Soc.*, **2009**, *131*, 4866-4871.
- (6) A. L. Goodwin, M. Calleja, M. J. Conterio, M. T. Dove, J. S. O. Evans, D. A. Keen, L. Peters, M. G. Tucker, *Science*, **2008**, *319*, 794-797.
- (7) A. Kondo, K. Maeda, *J. Solid State Chem.*, **2015**, *221*, 126-131.
- (8) F. Cacho-Baio, M. Etxeberria-Benavides, O. David, C. Téllez, J. Coronas, *ACS Appl. Mater. Interfaces*, **2017**, *9*, 20787-20796.